Use of the Kohonen Neural Network for Rapid Screening of Ex Vivo Anti-HIV Activity of Styrylquinolines

Jaroslaw Polanski,[†,‡] Fatima Zouhiri,[§] Laurence Jeanson,[‖] Didier Desmaële,[§] Jean d'Angelo,[§] Jean-François Mouscadet,[‖] Rafal Gieleciak,[‡] Johann Gasteiger,[⊥] and Marc Le Bret*,[†]

CNRS UMR 8532, LBPA, Ecole Normale Supérieure de Cachan, 61 avenue du Président Wilson, 94235 Cachan, France, Institute of Chemistry, University of Silesia, Szkolna 9, PL-40006-Katowice, Poland, Unité de Chimie Organique, CNRS UPRES A 8076, Centre d'Etudes Pharmaceutiques, 5 rue J.-B. Clément, Université de Paris Sud, 92296 Châtenay-Malabry, France, CNRS UMR 8532, Institut Gustave Roussy, PRII, 39 rue Camille Desmoulins, 94805 Villejuif, France, and Computer-Chemie-Centrum, Institute of Organic Chemistry, University of Erlangen-Nürnberg, Nägelsbachstrasse 25, D-91052 Erlangen, Germany

Using the Kohonen neural network, the electrostatic potentials on the molecular surfaces of 14 styrylquinoline derivatives were drawn as comparative two-dimensional maps and compared with their known human immunodeficiency virus (HIV)-1 replication blocking potency in cells. A feature of the potential map was discovered to be related with the HIV-1 blocking activity and was used to unmask the activity of further five analogues, previously described but whose cytotoxicity precluded an estimation of their activity, and to predict the activity of 10 new compounds while the experimental data were unknown. The measurements performed later turned out to agree with the predictions.

Introduction

Acquired immunodeficiency syndrome (AIDS) is essentially a viral disease and should be treated by antiretroviral agents.[1] The advent of combination antiretroviral therapy has made it possible to suppress the replication of human immunodeficiency virus (HIV)-1 in infected persons to such an extent that the virus becomes undetectable in the plasma for more than two years but seems to persist in peripheral blood mononuclear cells. This means that HIV-1 infection can be controlled but not eradicated with current treatments[2,3] using a combination of drugs reviewed in ref 4. It is then important to find new anti-HIV-1 agents. As it is very difficult to find a new compound from scratch, many research programs are limited to chemical substitutions on an existing active compound. As work goes on, a set of cognate compounds of known (in)activity are progressively recognized. For instance, at the present time, 19 styrylquinoline derivatives have been described.[5,6] At this point, we can follow either of two avenues of investigation. In the first approach, the binding site of the drugs on their molecular target can be characterized as accurately as possible at the atomic level using various physicochemical methods including in silico docking.[7,8] Integrase, the HIV-1 enzyme that catalyzes the insertion of retrotranscribed viral DNA into the cellular host genome, is probably a target since many styrylquinoline derivatives are potent inhibitors of the enzyme in vitro.

However, the in vivo activity does not depend solely on the inhibitory effect. In the HIV-1 integrase, the in vitro enzyme structure may differ from its structure in an infected cell where it is part of a multiproteinic complex. Moreover, cellular heterogeneities, localizations, and membrane permeabilities are just skipped over in an in vitro study, let alone in an in silico study. Therefore, to simulate the in vivo blocking effect in an infected human patient, ex vivo experiments are used, where cells are grown, infected with viruses, and then set in the presence of drug. In a second approach, followed here, the properties of the drugs themselves can be analyzed to find a rule enabling the screening of drugs that kill HIV-1 in cell culture.

Results

Chemical Compounds. The 19 styrylquinoline derivatives that were described in the literature[5,6] before this study are represented in Figure 1. The compounds are ordered according to the concentration required to achieve a 50% reduction of the viral load in the cell supernatant, IC_{50}. The IC_{50} (mM) is shown in italics under each formula. Compounds **1−11** are active and block the HIV-1 in cell culture. Compounds **12−14** are inactive. The blocking activity of **15−19** is masked by their cytotoxic effect.

In addition to the IC_{50}, two percentages, RV and *C*, are given under each formula to characterize the activity of the compound at 100 μM concentration. RV is residual virus expressed as a percentage of virus in nontreated cells. *C* is the percentage of dead cells and characterizes drug cytotoxicity. RV and *C* values were measured before this work but not reported in it.[5,6]

The compounds **20−29** in Table 1 are called new because their biological properties were still unknown when the computations were being performed. This was the case with **20** although its chemical synthesis has been earlier described.[6] All other new styrylquinolines **21−29** shown in Table 1 were basically elaborated

* To whom correspondence should be addressed. Tel: 33 1 47 40 59 97. Fax: 33 1 47 40 24 79. E-mail: mlebret@lbpa.ens-cachan.fr.
† Ecole Normale Supérieure de Cachan.
‡ University of Silesia.
§ Université de Paris Sud.
‖ Institut Gustave Roussy.
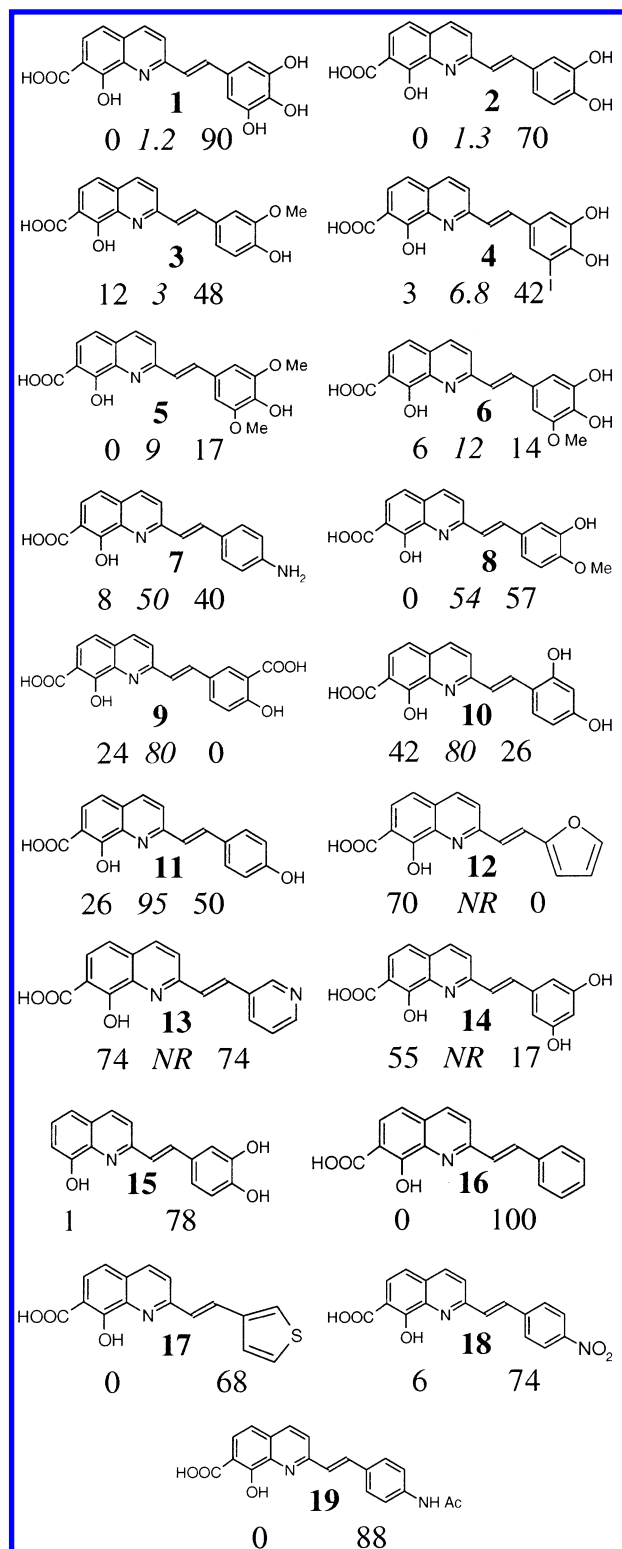⊥ University of Erlangen-Nürnberg.

Figure 1. Formulas and ex vivo activity of the styrylquinoline derivatives described in refs 5 and 6. Under each compound number (bold), three numbers characterize the ex vivo activity: RV (residual viruses in cell supernatant in the presence of 100 μM drug, expressed as a percentage of nontreated infected cells), IC$_{50}$ (the concentration required to achieve a 50% reduction of the viral load in the cell supernatant; NR, not reached, means that IC$_{50}$ is expected to be much larger than 100 μM), and C (percentage of dead cells in the presence of 100 μM drug). Compounds **1**−**11** are active and are sorted according to increasing IC$_{50}$ values; **12**−**14** are inactive. The activity of **15**−**19** is masked by their cytotoxicity, and only RV and C values are shown.
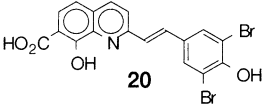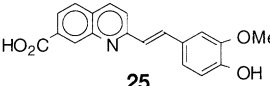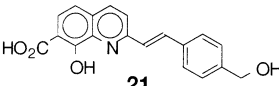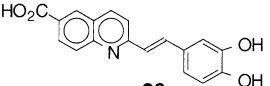
Scheme 1
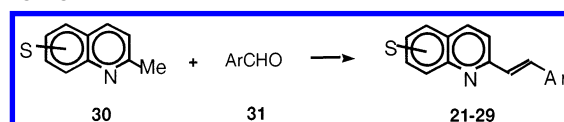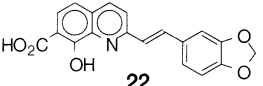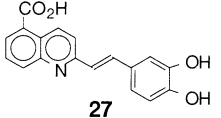
through Perkin type condensation between a 2-meth-ylquinoline moiety **30** and an aromatic aldehyde **31** (or aromatic ketal **48** in the case of **21**), followed by neutral or acidic hydrolysis (Scheme 1). Known 8-hydroxy-7-quinaldic acid (**33**),[9] which was used as the starting subunit in the syntheses of derivatives **21**−**23** and **29**, was prepared through Kolbe−Schmidt carboxylation of 8-hydroxyquinaldine **32**. Quinaldic acids **35**, **37**, **39**, **42**, and **44**, required for the syntheses of styrylquinolines **24**, **26**, **28**, **25**, and **27**, respectively, were synthesized by condensation of commercially available substituted anilines with crotonaldehyde under standard Doebner−Miller conditions. 8-Quinaldi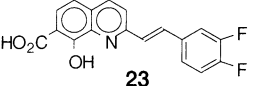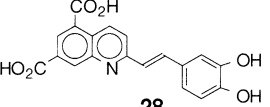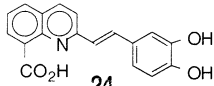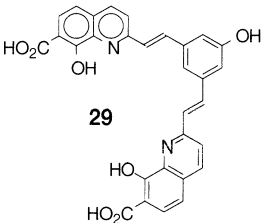c acid **35**,[10] 6-quinaldic acid (**37**),[11] and 5,7-quinaldinedicarboxylic acid **39** were thus prepared from anthranilic acid (**34**), 4-aminobenzoic acid **36**, and 5-aminoisophthalic acid **38**, respectively. 7-Quin-aldic acid (**42**) was obtained by acidic hydrolysis, using harsh conditions, of 7-trifluoromethylquinaldine (**41**),[12] itself prepared from 7-trifluoromethylaniline **40**. 5-Quin-aldic acid **44** was obtained as a 2:1 mixture with regio-isomer **42**, starting from 3-aminobenzoic acid **43**. Frac-tional crystallization then delivered pure quinaldine **44**[11] (Scheme 2). All aromatic aldehydes used are com-mercially available, with the exception of **46**, which was prepared in three steps from 5-hydroxyisophthalic acid **45**.[13] Acetal **48** was elaborated through NaBH$_4$ reduc-tion of commercially available terephthaldehyde mono-(diethyl acetal) **47** (Scheme 3).

The HIV blocking activity and cytotoxicity of the new compounds are shown in Table 1. Compounds **20**, **22**, and **24**−**28** are active ex vivo, but **21**, **23**, and **29** are inactive. Despite a favorable IC$_{50}$, **23** must be considered as inactive because of its high cytotoxicity (see RV and C values). The in vitro activity of the new compounds have also been measured using the methods described in the Experimental Section. Compounds **20**−**22** and **29** inhibit HIV-1 integrase in vitro in the micromolar range, **23** is not as good, and **24**−**28** have no effect below 100 μM. These results are intriguing; while **2** is active ex vivo and inhibits integrase in vitro, **24** and **29** have different and opposite behaviors: **24** is active ex vivo and inactive in vitro, and **29** is inactive ex vivo and active in vitro. Therefore, the new compounds do not make a homogeneous series in which the HIV blocking activity would be related to the ability to inhibit integrase in vitro. These experimental results were not known when the following computation work was started.

Maps of the Electrostatic Potentials. Using the Kohonen neural network,[14] it is possible to draw the electrostatic potentials on the molecular surfaces as a planar square map in such a way that no point is hidden[15] as described thoroughly in the Experimental Section. Moreover, the molecules have to be systemati-cally aligned.[16−21] This was done here by superimposing the carbon atoms 2, 3, 6, and 7 of the quinoline moieties as shown in Figure 2. The projection of points from the surfaces of the processed molecules into such a network allows comparing of those parts of the molecule surfaces

Table 1. HIV-1 Inhibitory Potencies and Cytotoxicity of Compounds **20−29**, Determined as Described in the Experimental Section

Compound	Antiviral activity		Cyto-toxicity	Compound	Antiviral activity		Cyto-toxicity
	RV^a	$IC_{50}{}^b$	C^c		RV^a	$IC_{50}{}^b$	C^c
20	13	30	8	**25**	17	20	30
21	55	110	17	**26**	4	20	0
22	4	10	40	**27**	5	50	0
23	2	30	91	**28**	5	15	0
24	0	12	0	**29**	100	NR^d	0

^{a} Residual viruses in cell supernatant in the presence of 100 μM drug, expressed as a percentage of nontreated infected cells. ^{b} Drug concentration (μM) at which 50% of the viruses are killed. ^{c} Percentage of dead cells in the presence of 100 mM drug. ^{d} Not reached.
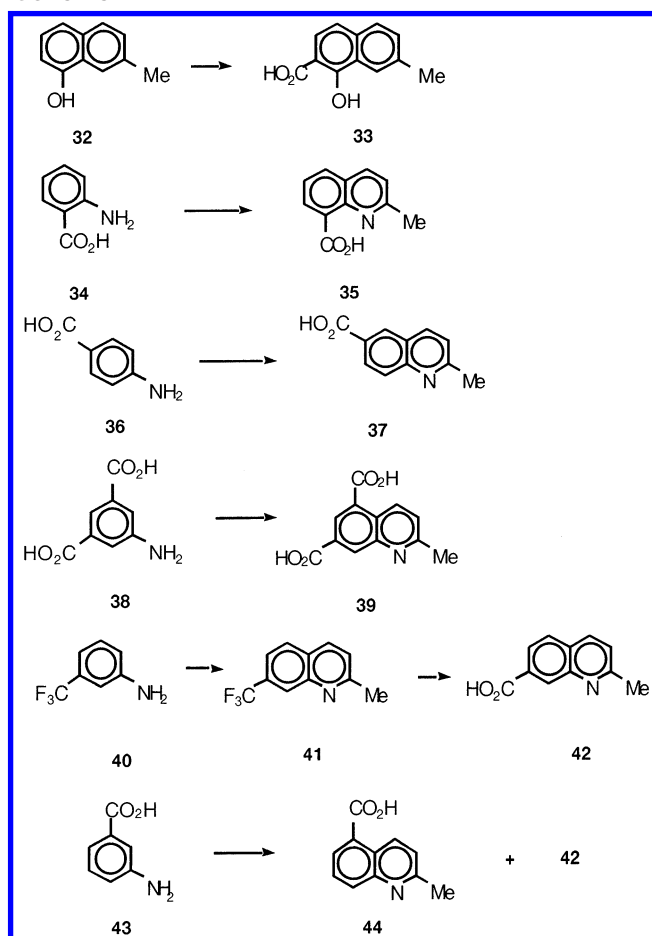
that can be superimposed. If the surfaces cannot be superimposed on the reference molecule (template), then the respective output neurons get no signal from the molecules processed. We indicated such neurons by a white color. It has to be emphasized that this approach for comparing molecular surface properties is an unsupervised learning process. Only the Cartesian coordinates of points on the molecular surface are used for training the neural network. The molecular electrostatic potential is only used for visualizing the results of the mapping of the surface points into the two-dimensional (2D) network. A neuron was colored by the electrostatic potential that existed at that point of the molecular surface that was mapped into this particular neuron.

These 2D electrostatic maps can easily be compared, with red indicating the most electronegative and purple the most electropositive areas. Because the quinoline moiety of the molecules remains unchanged, the patterns contain only a small number of empty neurons (white areas) and differ mainly in terms of their color profile.
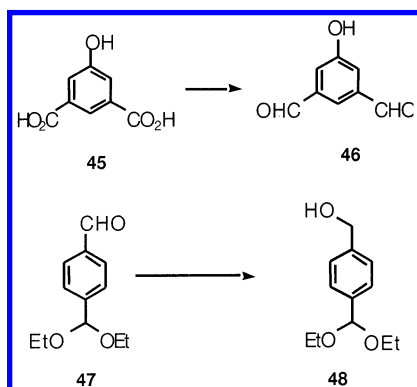
Through an extensive study of the comparative Kohonen maps of the different structural motifs of the molecules, we have found an interesting pattern that clearly differentiates active from inactive molecules. Figure 2a shows the average electrostatic map of the

inactive analogues **12−14**, and Figure 2b shows the corresponding one for active analogues **1−11**. Although there is no quantitative relationship between the size of the purple region and the RC value, analysis of the average profile clearly indicates a requirement for activity. Molecules with purple neurons in the encircled region contain an area with an electropositive potential and are inactive. Because the same quinoline motif is preserved in all molecules of the series, the difference must originate from the differences in the structure of the benzene part. In fact, by comparing the molecules, it was found that these differences result from a resonance effect enabling electron transfer between the two moieties. Electron-withdrawing groups in the quinoline moiety give it an electropositive character. However, the resonance electron transfer from the benzene counterpart can at least partly neutralize the electropositive character of this region. As expected, this effect is important for the electron-donating groups in the para position, in particular OH and OMe. In fact, there is not a single exception to this rule: all molecules containing electron-donating groups in this position are active. Conversely, those that are devoid of such groups are inactive. Therefore, our analysis revealed a key structural factor defining the ex vivo activity of the

Scheme 2

Scheme 3

Figure 2. Average maps of the electrostatic potentials for the inactive **12**−**14** (a) and active **1**−**11** (b) analogues. Molecular formula indicates the template motif used for the comparative Kohonen mapping (details in text). The molecules were aligned by superimposing the carbon atoms 2, 3, 6, and 7 of the quinoline moieties.
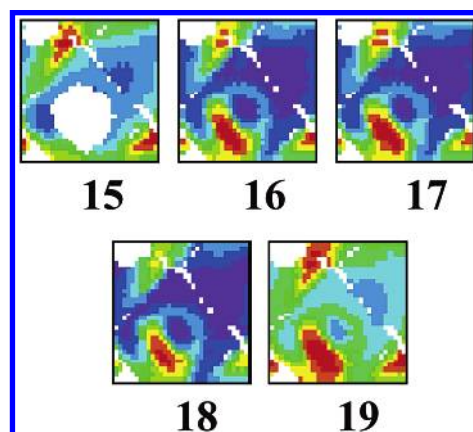
Figure 3. Maps of the electrostatic potentials for analogues **15**−**19**. Anti-HIV activity of these compounds cannot be estimated ex vivo due to high cytotoxicity. Color patterns of maps **16**−**18** correspond to inactive profiles, and **15** and **19** correspond to active profiles.

series and also gave a valuable clue for the design of additional analogues.

Figure 3 shows the maps of the molecules whose activity could not be estimated due to their high cytotoxicity. Interestingly, **15** and **19** display a pattern that defines them as active. Thus, provided that their level of activity is high enough, their use might be possible despite their cytotoxicity profile.

We next used a blind test procedure to compute the Kohonen plots of the new molecules **20**−**29**, before determining their experimental activity (Figure 4). The activity/inactivity predictions are shown below in each map as A (active) or IN (inactive). There is not a strict correspondence between the experimental numbers in Table 1 and the compound being qualified as A or IN. For instance, the compound **23** is so cytotoxic that it
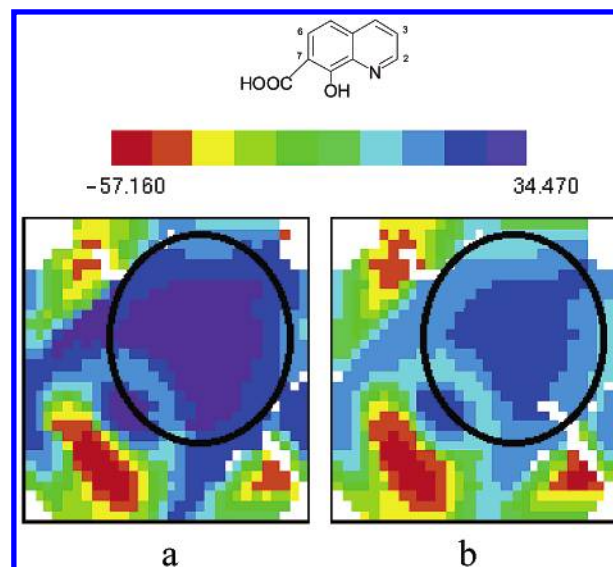
must be considered as inactive despite its RV value. The same argument holds for compounds **22** and **25**. Although their C value was smaller than that of **23**, they were not considered as truly active and they were qualified by a low case a. Predictions can also be ambiguous. As the rule for inactivity is the presence of purple neurons, **26**−**28** are predicted as active. However, it was felt that empty neurons in the critical region do not have the same value as blue ones. So, **26**−**28** were qualified A[?]. The results are summarized in Figure 4. The predictions are completely successful, i.e., the Kohonen patterns of the new analogues correlate nicely with their actual activity.

Discussion and Conclusion

Using Kohonen maps of electrostatic potential, a feature characterizing active compounds was extracted from the analysis of 14 compounds. The presence of a purple neuron in the circled region of the map makes

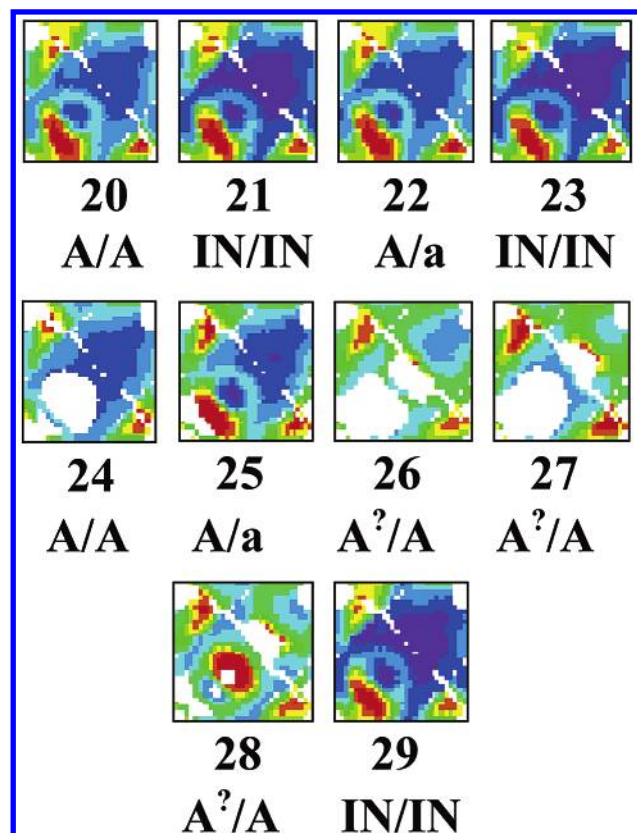**Figure 4.** Maps of the electrostatic potentials for new analogues **20**−**29**. The respective labels A (active) and IN (inactive) indicate the activity predicted from the estimation of the color profiles vs experimental activity (predicted/experimental). The maps of **24**−**28** contain empty neurons in the region encircled in Figure 2. The predictions are riskier and are labeled A[?]. Relatively low activity (a) was observed for analogues **22** and **25**.

the compound inactive. The criterion was applied to 10 new compounds and agreed with the experimental results. There was no exception. The compounds cannot be experimentally characterized just through their RV because of the very different cytotoxic effects. Unfortunately, no rule predicting the cytotoxicity emerged so far. Despite many efforts, no quantitative relationship could be found between the potential and the ex vivo activity.

The existence of a qualitative rule fitting the experimental ex vivo activity was unexpected because many different blocking mechanisms may be involved along the virus replicating cycle. Apparently, the new molecules form an heterogeneous series. Only for some of new molecules, the ex vivo activity is related to the ability to inhibit HIV-1 integrase in vitro. The new molecules can be clustered by the potential maps: (**20**, **24**), (**26**−**28**), (**22**, **25**), and (**21**, **23**, **29**), and this might be a clue to the physicochemical process involved in the anti-HIV activity. However, the existence of the rule, even though qualitative, shows that the involved processes must use the same feature in the electrostatic potential in some similar way.

Thus, we have shown that Kohonen maps of electrostatic potential represent a powerful tool for analyzing structure−activity data. This method helps elucidate the key molecular features governing the activity of novel HIV inhibitors and could correctly predict the

activity profiles of a set of newly synthesized compounds. We are now using this methodology to design additional anti-HIV agents to be developed soon.

Experimental Section

Computational Procedures. The three-dimensional (3D) structures of all molecules were generated by the 3D structure generator CORINA[22−24] and used without further optimization. The PEOE (partial equalization of orbital electronegativity) method[25] and its extension to conjugated systems[26] were used to calculate partial atomic charges. Residual electronegativity values were also obtained using the same procedures by considering the charge dependence of electronegativities using the PETRA program (parameter estimation for the treatment of reactivity applications).[27] The SURFACE program[27] uses the partial atomic charges to compute the Coulomb electrostatic potential on the molecular surface.

For the projection of the molecular electrostatic potential on the molecular surfaces, we used a Kohonen neural network consisting of a 2D arrangement of output neurons.[16−21] We used Cartesian coordinates (x,y,z) of the points sampled randomly from the molecular surface to define such a surface. As molecular surfaces are continuous surfaces, the plane of projection was selected to be also a continuous surface. Thus, we used a torus for this purpose, which has been cut along two perpendicular lines, and this cut surface has been spread into a plane. Each neuron, j, is then defined by three weights, w_{ji}. The competitive training of the network is based on the rule that each point, s, of the molecular surface is projected into that neuron, sc, that has weights, w_{ci}, that come closest to the Cartesian coordinates, x_{si}, of this point, s:

$$\text{out}_{sc} = \min[\sum_{i=1}^{3} (x_{si} - w_{ci})^2] \qquad (1)$$

A projection of the electrostatic potential value (MEP) from the surface points, s, into such a 2D arrangement of neurons, after calculating the average MEP value within this particular neuron and scaling these values into the respective colors, results in a so-called feature map.[16,19]

In fact, such a map illustrates the property (MEP) of a single molecule. As however, the weights of the Kohonen network contain the shape of the certain molecular surface, it can be used to compare the geometries of molecular surfaces of other molecules. In such a method, the trained Kohonen network is processing the signals coming from the surface of other molecule(s), i.e., the electrostatic potential of each input vector was projected through the network to obtain a series of comparative maps[16−21] both for the template molecule and each analyzed molecule.

Then, projecting of the respective electrostatic potential values from the surfaces of the processed molecules into such a network allows comparing of these parts of the molecule surfaces that can be superimposed. If the surfaces cannot be superimposed on the reference molecule (template), then the respective output neurons get no signal from the molecules processed. We indicated such neurons by a white color.

We used the KMAP[27] program to generate the Kohonen maps consisting of 30 × 30 neurons. All of the mentioned programs are available from J.G.[27]

Chemistry. Melting points were recorded on a capillary tube melting point apparatus and are uncorrected or by microthermal analysis on a Mettler FP5 apparatus. Infrared (IR) spectra were obtained as solid on a Fourier transform (FT) IR spectrometer Bruker Vector 22. The ^{1}H and ^{13}C NMR spectra were recorded on Bruker AC 200 P (200 and 50 MHz, for ^{1}H and ^{13}C, respectively) or Bruker ARX 400 (400 and 100 MHz). When diffuse, easily exchangeable protons were not listed. Recognition of methyl, methylene, methine, and quaternary carbon nuclei in ^{13}C NMR spectra rests on the *J*-modulated spin−echo sequence. Analytical thin-layer chromatography was performed on Merck silica gel 60F₂₅₄ glass precoated plates (0.25 mm layer). All liquid chromatography

separations were performed using Merck silica gel 60 (230–400 mesh ASTM). Ether was distilled from Na–benzophenone ketyl. Methanol was dried over magnesium and distilled. CH_2Cl_2 was distilled from calcium hydride, under a nitrogen atmosphere. All reactions were routinely conducted in glassware, which was flame-dried under a positive pressure of nitrogen. Organic layers were dried over anhydrous $MgSO_4$. Chemicals obtained from commercial suppliers were used without further purification.

Preparation of Quinaldic Acids. General Method A. To a refluxing solution of 1.0 equiv of amine in 6 N HCl (2 mL/mmol) was added dropwise, over a 2 h period, 1.2 equiv of crotonaldehyde. The resulting mixture was heated under reflux for 2 h. After it was cooled, aqueous ammonia was added to pH 3 and the mixture was extracted with CH_2Cl_2. The organic phase was washed with brine, dried over magnesium sulfate, and concentrated under vacuum. The crude product was recrystallized and dried in vacuo to give the respective acids.

5-Quinaldinecarboxylic Acid (44). Method A using **43** gave a 2:1 mixture of **44** and **42**. Recrystallization from ethanol afforded pure acid **44** in 26% yield as a white solid; mp >280 °C (dec) (lit.[11] mp 285 °C). IR (neat, cm^{-1}): 3500–2400, 1687, 1612, 1566. ^{1}H NMR (DMSO-d_6, 200 MHz): δ 9.15 (d, J = 8.8 Hz, 1H), 8.15 (d, J = 7.2 Hz, 1H), 8.11 (d, J = 8.4 Hz, 1H), 7.75 (dd, J = 8.4, 7.2 Hz, 1H), 7.50 (d, J = 8.8 Hz, 1H), 2.66 (s, 3H). ^{13}C NMR (DMSO-d_6, 50 MHz): δ 167.8 (C), 158.8 (C), 147.4 (C), 133.8 (CH), 132.2 (CH), 129.3 (CH), 128.1 (CH), 127.7 (C), 124.6 (C), 123.1 (CH), 24.6 (CH$_3$). Anal. ($C_{11}H_9NO_2$·HCl) C, H, N.

6-Quinaldinecarboxylic Acid (37). Method A using **36** gave acid **37** in 30% yield as white crystals; mp 270–272 °C (H_2O) (lit.[11] mp 259 °C). IR (neat, cm^{-1}): 3500–2400, 1706, 1645, 1605. ^{1}H NMR (DMSO-d_6, 200 MHz): δ 9.08 (d, J = 8.6 Hz, 1H), 8.87 (s, 1H), 8.45 (s, 2H), 7.95 (d, J = 8.6 Hz, 1H), 2.98 (s, 3H). ^{13}C NMR (DMSO-d_6, 50 MHz): δ 167.0 (C), 161.1 (C), 149.0 (C), 137.3 (CH), 130.5 (CH), 128.8 (CH), 128.4 (CH), 127.7 (C), 125.4 (C), 122.8 (CH), 25.0 (CH$_3$). Anal. ($C_{11}H_9NO_2$) C, H, N.

7-Trifluoromethylquinaldine (41). To a refluxing solution of 1.0 equiv of 3-trifluoromethylaniline (32.2 g, 0.20 mol) in 6 N HCl (100 mL), crotonaldehyde (20.2 g, 0.46 mol) was added dropwise over a 1 h period. The resulting mixture was heated under reflux for 2 h. After it was cooled, aqueous ammonia was added to pH 3 and the mixture was extracted with ether. The organic phase was washed with brine, dried over magnesium sulfate, and concentrated under vacuum. The crude product was distilled through a Vigreux column. A small, more volatile fraction of 5-trifluoromethylquinaldine precedes the main fraction of **41** (26.5 g, 63% yield) as a colorless liquid, which crystallized to a low melting point colorless solid on standing; bp 85–90 °C (0.1 Torr). ^{1}H NMR (CDCl$_3$, 200 MHz): δ 8.31 (broad s, 1H), 8.06 (d, J = 8.4 Hz, 1H), 7.85 (d, J = 8.6 Hz, 1H), 7.62 (dd, J = 8.4, 1.6 Hz, 1H), 7.35 (d, J = 8.6 Hz, 1H), 2.76 (s, 3H). ^{13}C NMR (CDCl$_3$, 50 MHz): δ 160.4 (C), 146.6 (C), 135.6 (CH), 130.9 (q, J = 32 Hz, C), 128.4 (CH), 126.4 (CH), 123.9 (q, J = 269 Hz, C), 123.7 (CH), 121.0 (CH), 25.1 (CH$_3$). Anal. ($C_{11}H_8F_3N$·1/4H_2O) C, H, N.

7-Quinaldinecarboxylic Acid (42). A mixture of **41** (10.0 g, 47.4 mmol) and 80% sulfuric acid was heated at 230 °C for 20 min. After it was cooled, 6 N sodium hydroxide was added until pH 12. The solid was filtered and washed with a small amount of water and ethanol. The filtrate was acidified with concentrated HCl until pH 3. After it stood for one night at room temperature, the mixture was filtered, and the solid was washed with water and dried under vacuum to give acid **42** (5.2 g, 59%) as a pinkish solid; mp 234–236 °C (H_2O). IR (neat, cm^{-1}): 3060–2200, 1685, 1605, 1558. ^{1}H NMR (DMSO-d_6, 200 MHz): δ 8.46 (s, 1H), 8.30 (d, J = 8.4 Hz, 1H), 8.00 (s, 2H), 7.50 (d, J = 8.4 Hz, 1H), 2.67 (s, 3H). ^{13}C NMR (DMSO-d_6, 50 MHz): δ 167.6 (C), 160.4 (C), 146.9 (C), 136.3 (CH), 131.8 (C), 130.5 (CH), 129.0 (C), 128.6 (CH), 125.3 (CH), 124.3 (CH), 25.2 (CH$_3$). Anal. ($C_{11}H_9NO_2$) C, H, N.

8-Quinaldinecarboxylic Acid (35). Method A using **34** gave acid **35** in 84% yield as white crystals; mp 156–157 °C (CHCl$_3$) (lit.[11] mp 151 °C). IR (neat, cm^{-1}): 3500–2400, 1699, 1617, 1579, 1513. ^{1}H NMR (CDCl$_3$, 200 MHz): δ 8.74 (d, J = 6.9 Hz, 1H), 8.27 (d, J = 8.2 Hz, 1H), 8.03 (d, J = 8.0 Hz, 1H), 7.67 (dd, J = 8.2, 6.9 Hz), 7.45 (J = 8.0 Hz, 1H). ^{13}C NMR (DMSO-d_6, 50 MHz): δ 166.7 (C), 159.5 (C), 144.2 (C), 139.4 (CH), 134.4 (CH), 133.7 (CH), 126.6 (CH), 126.5(C), 123.6 (CH), 123.4 (C), 24.7 (CH$_3$). Anal. ($C_{11}H_9NO_2$) C, H, N.

5,7-Quinaldinedicarboxylic Acid (39). Method A using 5-amino-isophthalic acid (**38**) gave acid **39** in 40% yield as ochre crystals. IR (neat, cm^{-1}): 3500–2400, 1704, 1649, 1601. ^{1}H NMR (DMSO-d_6, 200 MHz): δ 9.41 (d, J = 8.9 Hz, 1H), 8.82 (s, 1H), 8.65 (s, 1H), 7.83 (d, J = 8.9 Hz, H), 2.83 (s, 3H). ^{13}C NMR (DMSO-d_6, 50 MHz): δ 166.8, 165.8, 159.9, 143.3, 137.4, 131.8, 131.0, 129.4, 128.5, 126.9, 125.9, 21.7.

Condensation of Quinaldic Acid Derivatives with Aromatic Aldehydes. General Method B. To a solution of 1.0 equiv of **33** in acetic anhydride (3 mL/mmol) was added 4 equiv of aldehyde. The resulting mixture was heated under reflux for 16 h and concentrated in vacuo. The residue was dissolved in pyridine (4 mL/mmol), water (1 mL/mmol) was then added, and the reaction mixture was refluxed for 3 h. After it was cooled, the mixture was concentrated under reduced pressure. The residue was taken up into CH_2Cl_2 and filtered. The process was repeated with 2-propanol. The product was then thoroughly washed with 2-propanol and ether and dried in vacuo to provide the respective styryquinolines in 30–50% yields.

General Method C. To a solution of 1.0 equiv of the given quinaldic acid in acetic anhydride (3 mL/mmol) was added 4 equiv of aldehyde. The mixture was heated under reflux for 16 h and concentrated in vacuo. The residue was dissolved in 6 N sulfuric acid (4 mL/ mmol), and the resulting solution was heated under reflux for 3 h. After it was cooled 0 °C, 6 N potassium hydroxide was added until neutrality. The mixture was filtered and washed with water, 2-propanol, and finally ether. The solid was collected and taken up into water, and the suspension was refluxed for 1 h. The mixture was then filtered; the solid was recovered and dried under vacuum. The product was finally recrystallized from 2-propanol and dried in vacuo to provide the respective styryquinolines in 30–50% yields.

(*E*)-2-(2-Benzo[1,3]dioxol-5-yl-ethenyl)-8-hydroxy-7-quinolinecarboxylic Acid (22). Method B using piperonal afforded acid **22** in 32% overall yield as brick red solid; mp >215 °C (dec). IR (neat, cm^{-1}): 3500–2300, 1666, 1596, 1487, 1444. ^{1}H NMR (DMSO-d_6, 200 MHz): δ 8.38 (d, J = 8.7 Hz, 1H), 8.01 (d, J = 8.7 Hz, 1H), 7.84 (d, J = 16.2 Hz, 1H), 7.82 (d, J = 8.7 Hz, 1H), 7.48 (d, J = 16.2 Hz, 1H), 7.32 (d, J = 0.9 Hz, 1H), 7.20 (d, J = 8.7 Hz, 1H), 7.15 (dd, J = 7.8, 0.9 Hz, 1H), 6.95 (d, J = 7.8 Hz, 1H), 6.08 (s, 2H). ^{13}C NMR (DMSO-d_6, 50 MHz): δ 171.2, 160.1, 153.3, 148.2, 147.9, 138.1, 137.0, 136.0, 130.4, 130.2, 126.5, 124.1, 123.3, 121.0, 114.5, 111.7, 108.4, 105.7, 101.2. Anal. ($C_{19}H_{13}NO_5$·1/4H_2O) C, H, N.

(*E*)-2-[2-(3,4-Difluoro-phenyl)ethenyl]-8-hydroxy-7-quinolinecarboxylic Acid (23). Method B using 3,4-difluorobenzaldehyde afforded acid **23** in 78% overall yield as an orange solid; mp 225–230 °C (dec). IR (neat, cm^{-1}): 3500–2300, 1685, 1602, 1516, 1487. ^{1}H NMR (DMSO-d_6, 200 MHz): δ 8.34 (d, J = 8.2 Hz, 1H), 7.94 (d, J = 8.2 Hz, 1H), 7.95–7.76 (m, 3H), 7.65–7.45 (m, 3H), 7.29 (d, J = 8.4 Hz, 1H). ^{13}C NMR (DMSO-d_6, 100 MHz): δ 172.3 (C), 159.9 (C), 153.7 (C), 149.7 (dd, J = 240, 6 Hz, CF), 149.6 (dd, J = 259, 16 Hz, CF), 138.1 (C), 137.4 (d, J = 5 Hz, CH), 134.1 (dd, J = 5, 3 Hz, C), 133.0 (CH), 131.0 (C), 128.7 (CH), 126.4 (CH), 124.6 (CH), 121.9 (CH), 117.9 (CH), 115.8 (CH), 115.5 (dd, J = 26, 5 Hz, CH), 111.1 (C). Anal. ($C_{18}H_{11}F_2NO_3$·H_2O) C, H, N.

(*E*)-2-[2-(3,4-Dihydroxy-phenyl)ethenyl]- 5,7-quinolinedicarboxylic Acid (28). Method C using **39** and 3,4-dihydroxybenzaldehyde afforded diacid **28** as an ochre solid; mp >350 °C (dec). IR (neat, cm^{-1}): 3600–2300, 1713, 1627, 1589, 1522. ^{1}H NMR (DMSO-d_6, 200 MHz): δ 9.52 (d, J = 9.5

Hz, 1H), 8.99 (s, 1H), 8.64 (d, $J = 1.7$ Hz, 1H), 8.45 (d, $J = 9.5$ Hz, 1H), 8.15 (d, $J = 16.2$ Hz, 1H), 7.46 (d, $J = 16.2$ Hz, 1H), 7.21 (d, $J = 1.7$ Hz, 1H), 7.08 (dd, $J = 8.2, 1.7$ Hz, 1H), 6.87 (d, $J = 8.2$ Hz, 1H). ^{13}C NMR (DMSO-d_6, 50 MHz): δ 167.8, 166.9, 157.6, 148.0, 147.6, 146.1, 136.7, 135.2, 134.6, 131.1, 129.0, 128.6, 128.1, 128.0, 124.8, 123.0, 120.7, 116.4, 114.6. Anal. ($C_{19}H_{13}NO_6 \cdot H_2O$) C, H, N.

(*E*)-8-Hydroxy-2-[2-(4-hydroxymethyl-phenyl)ethenyl]-7-quinolinecarboxylic Acid (21). To a solution of **33** (1.60 g, 7.8 mmol) in acetic anhydride (25 mL) was added ketal **48** (5.00 g, 24.0 mmol). The resulting mixture was heated under reflux for 36 h and concentrated in vacuo. The residue was taken up in 6 N sulfuric acid (15 mL), and the reaction mixture was refluxed for 4 h. After it was cooled at 0 °C, 6 N potassium hydroxide was added until pH 3. The solid was filtered and washed with water and dried. The brown solid was collected and taken up into water, and the suspension was refluxed for 1 h. The mixture was then filtered and washed with 2-propanol and finally ether. The solid was recovered and dried under vacuum to give 760 mg of acid **21** in 75% yield as an orange solid; mp >300 °C (dec). IR (neat, cm^{-1}): 3500–2500, 1679, 1599, 1483, 1439. ^{1}H NMR (DMSO-d_6, 200 MHz): δ 8.42 (d, $J = 8.6$ Hz, 1H), 8.09 (d, $J = 8.6$ Hz, 1H), 7.93 (d, $J = 16.4$ Hz, 1H), 7.82 (d, $J = 8.3$ Hz, 1H), 7.70–7.60 (m, 2 H), 7.61 (d, $J = 16.4$ Hz, 1H), 7.45–7.35 (m, 2 H), 7.29 (d, $J = 8.6$ Hz, 4.51 (s, 2 H). ^{13}C NMR (DMSO-d_6, 50 MHz): δ 171.2 (C), 159.6 (C), 153.5 (C), 144.1 (C), 138.7 (CH), 136.8 (CH), 136.5 (C), 134.3 (C), 130.8 (C), 128.0–126.4 (5CH), 125.1 (CH), 121.5 (CH), 115.4 (CH), 111.6 (C), 62.6 (CH$_2$). Anal. ($C_{19}H_{15}NO_4 \cdot 1/2H_2O$) C, H, N.

(*E,E*)-3,5-Bis-[2-(7-carboxy-8-hydroxy-quinolin-2-yl)-ethenyl]-1-hydroxyphenyl (29). Method B using 3 equiv of **33** and 1 equiv of 5-hydroxy-benzene-1,3-dicarbaldehyde (**46**) afforded acid **23** in 47% overall yield as an orange solid; mp 239 °C (dec). IR (neat, cm^{-1}): 3500–2400, 1682, 1588, 1433, 1382. ^{1}H NMR (DMSO-d_6, 200 MHz): δ 8.43 (d, $J = 8.6$ Hz, 2H), 8.10 (d, $J = 8.6$ Hz, 2H), 7.88 (d, $J = 16.2$ Hz, 2H), 7.85 (d, $J = 8.9$ Hz, 2H), 7.65 (d, $J = 16.2$ Hz, 2H), 7.62 (s, 1H), 7.30 (d, $J = 8.9$ Hz, 2H), 7.12 (s, 2H). Anal. ($C_{30}H_{20}N_2O_7 \cdot H_2O$) C, H, N.

(*E*)-2-[2-(3,4-Dihydroxy-phenyl)ethenyl]-8-quinoline-carboxylic Acid (24). Method B using **35** and 3,4-dihydroxy-benzaldehyde afforded acid **24** as a dark red solid; mp 253–255 °C. IR (neat, cm^{-1}): 3550–2400, 1697, 1594, 1565, 1513, 1443. ^{1}H NMR (DMSO-d_6, 200 MHz): δ 9.50 (broad s, 1H), 9.10 (broad s, 1H), 8.60 (d, $J = 8.7$ Hz, 1H), 8.52 (d, $J = 7.1$ Hz, 1H), 8.25 (d, $J = 7.7$ Hz, 1H), 8.10 (d, $J = 7.7$ Hz, 1H), 7.74 (m, 2H), 7.21 (d, $J = 16.2$ Hz, 1H), 7.18 (s, 1H), 7.08 (d, $J = 8.1$ Hz, 1H), 6.80 (d, $J = 8.1$ Hz, 1H). ^{13}C NMR (DMSO-d_6, 50 MHz): δ 166.7 (C), 155.8 (C), 148.0 (C), 145.8 (C), 144.6 (C), 139.2 (CH), 138.7 (CH), 134.4 (CH), 133.4 (CH), 127.1 (C), 126.9 (C), 126.3 (CH), 123.2 (C), 122.7 (CH), 120.9 (CH), 120.4 (CH), 116.0 (CH), 114.5 (CH). Anal. ($C_{18}H_{13}NO_4 \cdot 1/3H_2O$) C, H, N.

(*E*)-2-[2-(3,4-Dihydroxy-phenyl)ethenyl]-6-quinoline-carboxylic Acid (26). Method B using **37** and 3,4-dihydroxy-benzaldehyde afforded acid **26** in 63% overall yield as a dark red solid; mp 283–285 °C. IR (neat, cm^{-1}): 3550–2400, 1690, 1585, 1514. ^{1}H NMR (DMSO-d_6, 200 MHz): δ 9.10 (broad s, 1H), 8.55 (s, 1H), 8.41 (d, $J = 8.5$ Hz, 1H), 8.17 (d, $J = 8.7$ Hz, 1H), 7.98 (d, $J = 8.7$ Hz, 1H), 7.84 (d, $J = 8.5$ Hz, 1H), 7.72 (d, $J = 16.2$ Hz, 1H), 7.08 (d, $J = 16.2$ Hz, 1H), 7.13 (s, 1H), 7.02 (d, $J = 7.7$ Hz, 1H), 6.80 (d, $J = 7.7$ Hz, 1H). ^{13}C NMR (DMSO-d_6, 50 MHz): δ 167.1, 158.1, 149.2, 147.3, 145.7, 137.9, 136.6, 130.6, 129.3, 128.4, 127.8 (2 C), 126.1, 124.6, 120.5 (2 C), 116.0, 114.2. Anal. ($C_{18}H_{13}NO_4 \cdot 1/2H_2O$) C, H, N.

(*E*)-2-[2-(3,4-Dihydroxy-phenyl)ethenyl]-5-quinoline-carboxylic Acid (27). Method B using **44** and 3,4-dihydroxy-benzaldehyde afforded acid **27** as brown solid; mp 330 °C (dec). IR (neat, cm^{-1}): 3550–2400, 1655, 1626, 1594, 1557. ^{1}H NMR (DMSO-d_6, 200 MHz): δ 9.35 (broad s, 1H), 8.18 (d, $J = 7.6$ Hz, 1H), 9.10 (broad s, 1H), 8.20 (m, 2H), 7.92 (d, $J = 7.7$ Hz, 1H), 7.75 (t, $J = 7.7$ Hz, 1H), 7.70 (d, $J = 16.0$ Hz, 1H), 7.15 (d, $J = 16.0$ Hz, 1H), 7.10 (s, 1H), 7.01 (d, $J = 7.6$ Hz, 1H),

6.79 (d, $J = 7.6$ Hz, 1H). ^{13}C NMR (DMSO-d_6, 50 MHz): δ 167.9, 156.2, 147.9, 147.1, 145.7, 135.6, 134.2, 133.5, 129.6, 128.7, 127.8 (2C), 125.3, 124.7, 120.9, 120.1, 116.0, 114.1. Anal. ($C_{18}H_{13}NO_4 \cdot 1/2H_2O$) C, H, N.

(*E*)-2-[2-(4-Hydroxy-3-methoxyphenyl)ethenyl]-7-quin-olinecarboxylic Acid (25). Method B using **42** and vanillin afforded acid **25** as brick red solid; mp 262–264 °C. IR (neat, cm^{-1}): 3400–2300, 1765, 1589, 1563. ^{1}H NMR (DMSO-d_6, 200 MHz): δ 8.51 (s, 1H), 8.40 (d, $J = 1.7$ Hz, 1H), 7.99 (s, 1 H), 7.87 (d, $J = 8.6$ Hz, 1H), 7.80 (d, $J = 16.5$ Hz, 1H), 7.35 (d, $J = 0.9$ Hz, 1H), 7.30 (d, $J = 16.5$ Hz, 1H), 7.16 (dd, $J = 8.2, 0.9$ Hz, 1H), 6.83 (d, $J = 8.2$ Hz, 1H), 3.86 (s, 3H). ^{13}C NMR (DMSO-d_6, 50 MHz): δ 167.0 (C), 156.9 (C), 148.0 (C), 145.8 (C), 137.0 (CH), 136.7, (CH) 132.1 (C), 129.3 (CH), 129.1 (C), 128.4 (CH), 127.5 (C), 125.3 (CH), 124.0 (CH), 122.0 (CH), 121.3 (CH), 115.7 (CH), 110.6 (CH), 55.8 (CH$_3$). Anal. ($C_{19}H_{15}$-NO$_4 \cdot 1/2H_2O$) C, H, N.

HIV-1 IN Assay. Recombinant full size HIV-1 IN was expressed and purified as previously described.[28] The process-ing assay was performed using U5 21-mer duplex correspond-ing to the sequence of the U5 HIV-1 long terminal repeats (LTR) extremity as DNA substrate. A 0.025 pmol amount of 32P-labeled DNA substrate was incubated in the presence of 1 pmol of integrase in a buffer containing 20 mM Hepes, pH 6.8, 20 mM NaCl, 0.5 mM dithiothreitol, and 7.5 mM MgCl$_2$ at 37 °C .[29] The reaction was stopped by adding 80 mL of a stop solution (0.3 M sodium acetate, 10 mM Tris, pH 7.5, and 1 mM ethylenediaminetetraacetic acid (EDTA)). The reaction products were phenol-extracted, precipitated with ethanol, and resuspended in 7 M urea. Products were separated on 18% polyacrylamide/7 M urea gels. Phosphorimages were recorded on a STORM 840TM Phosphorimager (Molecular Dynamics) and quantified using ImageQuant software.

Antiviral Assays. The lymphocyte cell line CEM was maintained in a RPMI-1640 (GIBCO Laboratories) supple-mented with 10% fetal calf serum. Hela and Hela-CD4$^+$-βGal (P4) cells were grown in Dulbecco's modified Eagle's medium with 10% fetal calf serum and 0.5 mg/mL Geneticin. Cell-free viral supernatants were obtained by transfection of Hela cells with HIV-1 PLN4-3 genomic clone. Cells were plated in triplicate on 96 well plates (100 μL) and infected with cell-free virus. Viral supernatants were removed 2 h after infection, and drugs dissolved in dimethyl sulfoxide were added in fresh medium. After 72 h, supernatants were used to infect P4 cells. P4 cells were incubated for 24 h and subsequently lysed in a phosphate buffer containing 50 mM 2-mercaptoethanol, 10 mM MgSO$_4$, 25 mM EDTA, 0.125% NP40. A 20 μL amount of lysate was incubated with 100 μL of CPRG-containing buffer. The red staining intensity was quantified on a multiscan photom-eter at 570 nm. Cell viability was estimated by the MTT (Sigma) assay. A 20 μL amount of a solution of MTT (7.5 mg/mL) in phosphate buffer was added to each well of the microtiter trays. The plates were further incubated at 30 °C in a CO$_2$ incubator for 4 h. Solubilization of the formazan crystals was achieved by adding 100 mL of 10% sodium dodecyl sulfate and 10 mM HCl. Absorbances were read in a multiscan photometer at 570 nm.

References

(1) Ho, D. D.; Neumann, A. U.; Perelson, A. S.; Chen, W.; Leonard, J. M.; Markowitz, M. Rapid turnover of plasma virions and CD4 lymphocytes in HIV-1 infection. *Nature* **1995**, *373*, 123–126.
(2) Zhang, L.; Ramratnam, B.; Tenner-Racz, K.; He, Y.; Vesanen, M.; Lewin, S.; Talal, A.; Racz, P.; Perelson, A.; Korber, B.; Markowitw, M.; Ho, D. Quantifying residual HIV-1 replication in patients receiving combination antiretroviral therapy. *N. Engl. J. Med.* **1999**, *340*, 1605–1613.

(3) Furtado, M.; Callaway, D.; Phair, J.; Kunstman, K.; Stanton, J.; Macken, C.; Perelson, A.; Wolinsky, S. Persistence of HIV-1 transcription in peripheral-blood mononuclear cells in patients receiving potent antiretroviral therapy. *N. Engl. J. Med.* **1999**, *340*, 1614−1622.

(4) De Clercq, E. Toward improved anti-HIV chemotherapy: therapeutic strategies for intervention with HIV infections. *J. Med. Chem.* **1995**, *38*, 2491−2517.

(5) Mekouar, K.; Mouscadet, J. F.; Desmaële, D.; Subra, F.; Leh, H.; Savouré, D.; Auclair, C.; d'Angelo, J. Styrylquinoline derivatives: a new class of potent HIV-1 integrase inhibitors that block HIV-1 replication in CEM cells. *J. Med. Chem.* **1998**, *41*, 2846−2857.

(6) Zouhiri, F.; Mouscadet, J. F.; Mekouar, Kh.; Desmaële, D.; Savouré, D., Leh, H.; Subra, F.; Le Bret, M.; Auclair, C.; d'Angelo, J. Structure−activity relationships and binding mode of styrylquinolines as potent inhibitors of HIV-1-integrase and replication of HIV-1 in cell culture. *J. Med. Chem.* **2000**, *43*, 1533−1540.

(7) Ouali, M.; Laboulais, C.; Leh, H.; Gill, D.; Desmaële, D.; Mekouar, K.; Zouhiri, F.; d'Angelo, J.; Auclair, C.; Mouscadet, J. F.; Le Bret, M. Modeling of the inhibition of retroviral integrases by styrylquinoline derivatives. *J. Med. Chem.* **2000**, *43*, 1949−1957.

(8) Ouali, M.; Laboulais, C.; Leh, H.; Gill, D.; Xhuvani, E.; Zouhiri, F.; Desmaële, D.; d'Angelo, J.; Auclair, C.; Mouscadet, J. F.; Le Bret, M. Tautomers of styrylquinoline derivatives containing a methoxy substituent: computation of their population in aqueous solution and their interaction with RSV integrase catalytic core. *Acta Biochim. Pol.* **2000**, *47*, 11−22.

(9) Meek, W. H.; Fuschman, C. H. J. Carboxylation of substituted phenols in N, N-dimethylamide solvents at atmospheric pressure. *J. Chem. Eng. Data* **1969**, *14*, 388−391.

(10) Porai-Koshits, B. A.; Efros, L. S.; Vertkina, V. N.; Lutsenko, V. V. Preparation of derivatives of quinaldine from aromatic amines and vinyl ethers. *Zh. Obshchei Khim.* **1954**, *24*, 895−898; *Chem. Abstr.* **1955**, *49*, 8280.

(11) Doebner, O.; von Miller, W. Ueber Chinaldincarbonsäuren. *Chem Ber.* **1884**, *17*, 938−945.

(12) Gilman, H.; Blume, D. 5- and 7-Trifluoromethylquinolines. *J. Am. Chem. Soc.* **1943**, *65*, 2467−2468.

(13) Provent, C.; Chautemps, P.; Gellon, G.; Pierre, J.-L. Double Wittig reactions with 4-carboxybutylidene triphenylphosphorane as the key step in the synthesis of benzene derivatives metadisubstituted with ω,ω'-difunctionalized six carbon chains. *Tetrahedron Lett.* **1999**, *37*, 1393−1396.

(14) Kohonen, T. *Self-Organization and Associative Memory*, 3rd ed.; Springer-Verlag: Berlin, 1989.

(15) Anzali, S.; Barnickel, G.; Krug, M.; Sadowski, J.; Wagener, M.; Gasteiger, J.; Polanski, J. The comparison of geometric and electronic properties of molecular surfaces by neural networks: application to the analysis of corticosteroid-binding globulin activity of steroids. *J. Comput.-Aided Mol. Des.* **1996**, *10*, 521−534.

(16) Gasteiger, J.; Li, X.; Rudolph, Ch.; Sadowski, J.; Zupan, J. Representation of Molecular Electrostatic Potentials by Topological Feature Maps, *J. Am. Chem. Soc.* **1994**, *116*, 4608−4620.

(17) Polanski, J.; Gasteiger, J.; Wagener, M.; Sadowski, J. The comparison of molecular surfaces by neural networks and its application to quantitative structure activity studies. *Quant. Struct.-Act. Relat.* **1998**, *17*, 27−36.

(18) Anzali, S.; Gasteiger, J.; Holzgrabe, U.; Polanski, J.; Teckentrup, A.; Wagener, M. The use of self-organizing neural networks in drug design. *Persp. Drug Discovery Des.* **1998**, *9/10/11*, 273−299.

(19) Zupan, J.; Gasteiger, J. *Neural Networks in Chemistry and Drug Design*; Wiley-VCH: Weinheim, 1999; pp 317−336.

(20) Polanski, J.; Walczak, B. The comparative molecular surface analysis (COMSA): a novel tool for molecular design. *Comput. Chem.* **2000**, *24*, 615−625.

(21) Polanski, J.; Jarzembek, K.; Gasteiger J. Self-organizing neural networks for screening and development of novel artificial sweetener candidates. *Comb. Chem. High Throughput Screening Rev.* **2000**, *3*, 481−495.

(22) Sadowski, J.; Rudolph, C.; Gasteiger, J. The Generation of 3D-Models of Host-Guest Complexes. *Anal. Chim. Acta* **1992**, *265*, 233−241.

(23) Gasteiger, J.; Rudolph, C.; Sadowski, J. Automatic Generation of 3D-Atomic Coordinates for Organic Molecules. *Tetrahedron Comput. Methodol.* **1992**, *3*, 537−547.

(24) Sadowski, J.; Gasteiger, J. From Atoms and Bonds to Three-Dimensional Atomic Coordinates: Automatic Model Builders. *Chem. Rev.* **1993**, *93*, 2567−2581.

(25) Gasteiger, J.; Marsili, J. Iterative Partial Equalization of Orbital Electronegativity − A Rapid Access to Atomic Charges. *Tetrahedron* **1980**, *36*, 3219−3228.

(26) Gasteiger, J.; Saller, H. Calculation of the Charge Distribution in Conjugated Systems by a Quantification of the Resonance Concept. *Angew. Chem., Int. Ed. Engl.* **1985**, *24*, 687−689.

(27) Gasteiger, J.; et al. For the information, see http://www2.chemie.uni-erlangen.de/software.

(28) Leh, H.; Brodin, P.; Bischerour, J.; Deprez, E.; Tauc, P.; Brochon, J. C.; LeCam, E.; Coulaud, D.; Auclair, C.; Mouscadet, J. F. Determinants of Mg^{2+}-dependent activities of recombinant human immunodeficiency virus type 1 integrase. *Biochemistry* **2000**, *39*, 9285−9294.

(29) Brodin, P.; Pinskaya, M.; Buckle, M.; Parsch, U.; Romanova, E.; Engels, J.; Gottikh, M.; Mouscadet, J. F. Disruption of HIV-1 integrase-DNA complexes by short 6-oxocytosine-containing oligonucleotides. *Biochemistry* **2002**, *41*, 1529−1538.

JM020845G